

AFML-TR-77-233

2

LEVEL

ADA058045

EVALUATION OF A CRACK-GROWTH GAGE FOR MONITORING
POSSIBLE STRUCTURAL FATIGUE-CRACK GROWTH

AD No.

DDC FILE COPY

Metals Behavior Branch
Metals and Ceramics Division

February 1978

TECHNICAL REPORT AFML-TR-77-233

DDC
RECEIVED
AUG 28 1978
B

Final Report for Period May 1977 to September 1977

Approved for public release; distribution unlimited.

AIR FORCE MATERIALS LABORATORY
AIR FORCE WRIGHT AERONAUTICAL LABORATORIES
AIR FORCE SYSTEMS COMMAND
WRIGHT-PATTERSON AIR FORCE BASE, OHIO 45433

78 08 21 049


NOTICE

When Government drawings, specifications, or other data are used for any purpose other than in connection with a definitely related Government procurement operation, the United States Government thereby incurs no responsibility nor any obligation whatsoever; and the fact that the government may have formulated, furnished, or in any way supplied the said drawings, specifications, or other data, is not to be regarded by implication or otherwise as in any manner licensing the holder or any other person or corporation, or conveying any rights or permission to manufacture, use, or sell any patented invention that may in any way be related thereto.

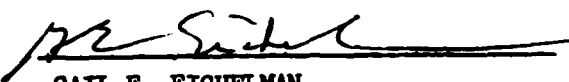
This report has been reviewed by the Information Office (OI) and is releasable to the National Technical Information Service (NTIS). At NTIS, it will be available to the general public, including foreign nations.

This technical report has been reviewed and is approved for publication.


A. F. Grandt, Jr., Project Engineer


N. E. Ashbaugh, Project Engineer

FOR THE COMMANDER


GAIL E. EICHELMAN
Actg. Chief, Metals Behavior Branch
Metals & Ceramics Division

"If your address has changed, if you wish to be removed from our mailing list, or if the addressee is no longer employed by your organization please notify AFML/LLN _____, W-PAFB, OH 45433 to help us maintain a current mailing list".

Copies of this report should not be returned unless return is required by security considerations, contractual obligations, or notice on a specific document.

UNCLASSIFIED

SECURITY CLASSIFICATION OF THIS PAGE (When Data Entered)

REPORT DOCUMENTATION PAGE		READ INSTRUCTIONS BEFORE COMPLETING FORM
1. REPORT NUMBER AFML TR-77-233	2. GOVT ACCESSION NO.	3. RECIPIENT'S CATALOG NUMBER
4. TITLE (and Subtitle) EVALUATION OF A CRACK-GROWTH GAGE FOR MONITORING POSSIBLE STRUCTURAL FATIGUE-CRACK GROWTH.	5. TYPE OF REPORT & PERIOD COVERED Final Report, May 1977 - September 1977	
7. AUTHOR(s) N. E. Ashbaugh, Systems Research Laboratories A. F. Grandt, Jr., Air Force Materials Laboratory	8. CONTRACT OR GRANT NUMBER(s) F33615-76-C-5191	
9. PERFORMING ORGANIZATION NAME AND ADDRESS Systems Research Laboratories & Air Force Materials Laboratory Wright-Patterson Air Force Base, Ohio 45433	10. PROGRAM ELEMENT, PROJECT, TASK AREA & WORK UNIT NUMBERS Project 2307 (12) P1 Task 2307P1 Work Unit 2307P102	
11. CONTROLLING OFFICE NAME AND ADDRESS Air Force Materials Laboratory (AFML/LLN) Air Force Wright Aeronautical Laboratories Wright-Patterson Air Force Base, Ohio 45433	12. REPORT DATE February 1978	
14. MONITORING AGENCY NAME & ADDRESS (if different from Controlling Office) (12) 46p.	13. NUMBER OF PAGES 40	
	15. SECURITY CLASS. (of this report) Unclassified	
16. DISTRIBUTION STATEMENT (of this Report) Approved for public release; distribution unlimited.		
17. DISTRIBUTION STATEMENT (of the abstract entered in Block 20, if different from Report)		
18. SUPPLEMENTARY NOTES		
19. KEY WORDS (Continue on reverse side if necessary and identify by block number) Crack Gage Fatigue Crack Growth Fracture (Materials) Fatigue Loads Structural Damage		
20. ABSTRACT (Continue on reverse side if necessary and identify by block number) The results of an experimental and analytical investigation on the use of a precracked coupon mounted onto a structure for monitoring the effect of service loads upon fatigue crack growth in the structure are discussed. The precracked coupon or "gage" is a simple device which provides a convenient means for determining the potential damage in a structure since the gage takes into account the mechanics of crack growth. Experimental results are reported for gages made from two aluminum alloys and having two types of crack		

DD FORM 1473 EDITION OF 1 NOV 65 IS OBSOLETE

UNCLASSIFIED

SECURITY CLASSIFICATION OF THIS PAGE (When Data Entered)

340 400

18 08 21 049

LB

next page

UNCLASSIFIED

SECURITY CLASSIFICATION OF THIS PAGE(When Data Entered)

geometries. These gages contained either a center crack or a single crack at the edge of a hole. The effect of the load amplitude upon the growth of the crack in the gage as a function of the crack growth in the structure was investigated. All tests were conducted under constant-amplitude cyclic load. The theoretical model is developed to predict the correlation between the growth of the cracks in the gage and in the structure. Two areas of major importance in the analysis are the load transfer from the structure through the ends of the crack gage and the crack-propagation law for the crack growth in the gage and in the structure. Comparison of the analyses and the experimental results is made.

UNCLASSIFIED

SECURITY CLASSIFICATION OF THIS PAGE(When Data Entered)

FOREWORD

This research was conducted in the Metals Behavior Branch, Metals and Ceramics Division, Air Force Materials Laboratory, Wright-Patterson Air Force Base, Ohio under Project No. 2307, "Failure Prediction in Metals", Task No. 2307P1, Work Unit No. 2307P102 with Dr. A. F. Grandt, Jr., as project engineer and AF Materials Laboratory contract F33615-76-C-5191 with Dr. N. E. Ashbaugh, Systems Research Laboratories as project engineer.

In the testing portion of this investigation, considerable support was provided by James G. Paine who bonded the many strain gages and the crack gages onto the test specimens and George F. Mornhinweg who precracked the gages and structural components and tested the specimens. Appreciation is also extended to Dennis E. Macha for his effort in making the laser-interferometric measurements.

AFML-TR-77-233		
DATE	BY	APPROVED
		<input checked="" type="checkbox"/>
CLASS.		<input type="checkbox"/>
EXTENSION		<input type="checkbox"/>
BY _____		
DISTRIBUTION/AVAILABILITY STATEMENTS		
Dist. AVAIL. and/or SPECIAL		
A		

TABLE OF CONTENTS

SECTION		PAGE
I	INTRODUCTION	1
II	EXPERIMENTAL	2
	1. Specimen Configuration and Test Matrix	2
	2. Crack-Growth Behavior	3
	3. Evaluation of Test Configuration	5
	4. Test Results	7
III	PREDICTIVE MODEL	8
IV	DISCUSSION OF RESULTS	14
V	SUMMARY AND CONCLUSIONS	18
	REFERENCES	20

LIST OF ILLUSTRATIONS

FIGURE		PAGE
1	Test Spec Configuration or Configuration of TS	25
2	Plot of Predicted Crack Growth Behavior from a Best Fit to the Experimental Data and an Adjusted Fit to the Data	26
3	Comparison of Crack-Length Results for Two Specimens Having Equivalent Initial Crack Lengths and Being Tested Under Different Load Amplitudes	27
4	Experimental Data and Theoretical Predictions for Structural Crack Growth Versus Gage Growth for Two Specimens Having Different Initial Crack Lengths	28
5	A Replot of the Test Data in Figure 2 After Elimination of the Dependence Upon the Number of Cycles: (a) Test 3 With Nominal Stress Range of 93.1 MPa and (b) Test 4 With Nominal Stress Range of 124 MPa	29
6	Plot of Structural Crack Length Versus Gage Crack Length for Specimens With Gages Made from 2024-T3 Al	31
7	Cumulative Effect of Additional Compliance Terms in the Load-Transfer Function Upon the Prediction of Structural Crack Length Versus Gage Crack Length	32
8	Comparison of the Predicted Dimensionless K --Equivalent to the Geometric Correction Factor--With the Dimensionless K Obtained from the Experimental Data on Structural Crack Growth	33
9	Comparison of the Predicted Dimensionless K --Equivalent to the Load-Transfer Function--With the Dimensionless K Obtained from the Experimental Data on Gage Crack Growth	34
10	Experimental Crack-Growth Data Indicating Both the Reproducibility and the Lack of Dependence Upon Load Amplitude of the Gage Response	35
A1	Crack Growth Rate for 2219-T851 Aluminum	38
A2	Crack Growth Rate for 7075-T6 Aluminum	39
A3	Crack Growth Rate for 2024-T3 Aluminum	40

SECTION I
INTRODUCTION

It is well known that a fleet of identical structures may be subjected to widely differing load histories during their service life. The service loading may differ from fleet member to fleet member and it may differ from the design spectrum for the structure. Thus, it is often extremely important to track the use of individual structures. The USAF has, for example, requirements for a tail-number tracking system of USAF aircraft (References 1-3). The intent of this tracking system is to measure and record load histories of service aircraft. Then the relative severity of the load histories on potential crack growth must be determined for the individual aircraft. Such requirements are, of course, not new and many techniques have been suggested for monitoring and recording loads--including pilot logs, VGH recorders, acoustic emission, and both electrical and mechanical devices for recording strains (References 4-7). Common to most of these techniques is the need for reducing the information collected into a load history and then performing a crack-growth analysis with the use of conventional fracture-mechanics techniques. Such a procedure for reducing field-collected data to crack-growth response becomes very complicated and cumbersome and involves a considerable expense and introduces possibilities for errors. This report describes an alternate approach for monitoring and determining the severity of service loads on the extension of pre-existent cracks which are assumed to be in the structure.

The approach discussed here consists of mounting a precracked coupon onto the structure. Loads induced in the structure will cause the crack in the coupon to grow. It is proposed that this measurable crack growth in the coupon can be related to extension of a structural flaw. The crack-gage concept for tracking fleet loads has been discussed by several authors, both in the context of crack initiation (Reference 8) and crack growth (References 9-11). The results of experiments which were designed for the preliminary evaluation of this concept are discussed in this report.

1
68 08 21 049

SECTION II

EXPERIMENTAL

Many variables are involved in evaluating the potential of the crack gage for determining damage in a structure. In the present study damage was considered to be the growth of a pre-existing flaw in the structure. This consideration was based upon USAF Document MIL-A-83444 which specifies design and size requirements for assumed pre-existing cracks in an aircraft structure. Some of the variables which apply to the structure and gage are: materials, crack geometry, environment, loading history, manner in which the gauge is attached, and location of the gage. For the experimental investigation, the prime objectives were the determination of reproducibility of data obtained from a crack gage and the effect of cyclic-load amplitude upon the relationship between crack length in the structure and that in the gage.

1. SPECIMEN CONFIGURATION AND TEST MATRIX

The structural component was a 5.08-cm-wide (2-in.), 0.61-cm-nominally thick (0.24-in.) strip, and the attached gage was 2.54-cm-wide (1-in.) and 0.079-cm nominally thick (0.031-in.) having an effective 3.81-cm (1.5-in.) gage length. The test configuration of the gage and structural component and the nominal dimensions are shown in Figure 1.

The test matrix for the experiments is given in Table 1. In general, two aluminum alloys were used for the gage. Two gage crack geometries were investigated (a center-cracked (CC) gage and a single-cracked hole (SCH) in the gage). For the structural component only one material and crack geometry was used. Tests 2 and 3 essentially involved duplicate initial crack geometries run at approximately the same load amplitude. In Test 4 the same initial crack geometry was tested at a higher load. Test 1 was run to determine the effects of changing the initial crack lengths. In Tests 6 and 7 a different gage material was used and a different crack geometry investigated.

2. CRACK-GROWTH BEHAVIOR

The material chosen for the structural component was 2219-T851 Al since it is a representative airframe material and since dogbone specimens were readily available. Two materials which were in stock were selected for the crack gage (2024-T3 Al sheet and Alclad 7075-T6 Al sheet). To permit analysis of the test-specimen results, baseline crack-growth data on these materials were obtained. Single-edge-notch (SEN) and center-cracked (CC) specimens of 2219-T851 (0.61-cm nominal thickness and 5.08-cm-wide) were tested under several constant-amplitude load levels. The orientation of the crack growth in these two types of specimens was LT, i.e., the crack surface was normal to the rolling direction (L) and the crack propagated in the transverse direction (T). CC specimens of 2024-T3 and 7075-T6 (0.079-cm nominal thickness and 2.54-cm wide) were tested under several constant-amplitude load levels. The orientation of crack growth in 2024-T3 and 7075-T6 was LT and TL, respectively. In all baseline crack-growth tests, the ratio of minimum load to maximum load (R) was 0.1.

A least-squares-fit parabola to successive sets of five data points (crack length vs number of cycles) was used to obtain the slope for crack-growth rate and the crack length for the range of the stress-intensity factor, ΔK . Then a linear regression on log-log scale plot of the results for crack-growth rate as a function of ΔK was applied to obtain the constants (denoted by C and m) for the Paris' crack growth law. Values of these constants for the structure and gage materials are presented in Table 2 and labeled "Experimental." From the experimental data, the valid ranges of ΔK (in $\text{MN m}^{-3/2}$) for the application of the constants are: $4.8 < \Delta K < 35$ for 2219-T851, $6.3 < \Delta K < 27$ for 7075-T6, and $5.6 < \Delta K < 30$ for 2024-T3. Plots of the reduced crack growth data for the structural material and the two-gage materials are shown in Appendix A. Note that the units for crack growth rate is in./cycle and for ΔK is $\text{psi } \sqrt{\text{in}}$. Thus the constants in the equation of the best fit line which is given of each plot are in units of in., lb., and cycles. The experimental values of the constants in Table 2 are obtained when units are converted to meters, Newtons, and cycles. In order to obtain the

largest range of ΔK in the test specimens and to allow application of the crack-growth law, the final precracking of the CC cracks in the gages and the SCH cracks in the structure was performed at $\Delta K = 6.6 \text{ MN m}^{-3/2}$.

A set of adjusted constants is also presented in Table 2. The adjusted values of C were obtained from a least-squares fit of the experimental data for 7075-T6 and 2024-T3, with $m = 2.855$ (the exponent for 2219-T851). A comparison of the predicted crack growth behavior which is obtained from the experimental values and the adjusted values of C and m is shown in Figure 2. Note that the change in predicted crack growth rate when the adjusted values are used instead of the experimental values is small for values of ΔK within the range of the experimental data. The application of the adjusted values of C and m is discussed in a subsequent section on the predictive model.

An adhesive was used to mount the gage onto the structural component. It was decided that bonding the gage onto the structure would be preferable to using rivets, which in a real structure would introduce additional holes and, in turn, could be potential sites for flaws. The choice of adhesive was based upon ease of application, availability, and reliability under laboratory conditions. Four available adhesives were used to attach uncracked gage coupons to the dogbone structure. These trial specimens were tested under conditions similar to those expected for the actual specimens. The adhesive which provided the most reliable bonding in laboratory usage and which was subsequently employed for all test specimens was Hysol Aerospace Adhesive EA 9628 Tape. It should be noted that it was beyond the scope of this investigation to evaluate adhesives for long-term usage in field applications. The metal surfaces to be bonded were cleaned and prepared using the same techniques as those used for the application of strain gages. The recommended conditions for the curing cycle were 0.17 MPa (24 psi) at 121°C (250°F) for one hour. However, since the preliminary study of the adhesives had indicated that adequate bonding was obtained at 0.17 MPa at 121°C for 1/2 hour, all test specimens underwent this 1/2-hour curing cycle.

In order to maintain a uniform unbonded length on the crack gage, a 0.013-cm-thick (0.005 mil) and 3.81-cm-long (1.5-in.) Teflon strip was placed between the gage and the structural component. Thus, the bonded areas on the gage had a straight edge under the gage and were ~ 2.54-cm long (1-in.).

3. EVALUATION OF TEST CONFIGURATION

In order to develop a model for the test specimens shown in Figure 1, the characteristics of the load transfer into the gage and the possible effects of the gage upon the nominal stress field around the structural crack were evaluated. Strain gages were attached to a sample test specimen which had an uncracked coupon mounted onto it to simulate a crack gage, and which had no hole or crack in the structural component. Since the uncracked coupon was stiffer than a cracked gage, the limiting conditions for load transfer into a gage and the effects upon the nominal stress in the vicinity of the crack in the structural component were maximized. Pairs of strain gages were placed on top of the coupon, on top of the structural component beside the coupon, on the bottom of the structural component beneath the coupon, and on the top and bottom of the structural component at the location of the structural crack. These strain-gage locations are indicated in Figure 1.

Three uncracked specimen configurations were tested. The first configuration was to simulate test specimens where only the adhesive was used to attach the coupon to the structural component. The second configuration was identical to the first, except that two rivets in addition to the adhesive were placed along the edge of each bonded area. The third configuration was similar to first, except that the structural component was approximately twice as thick.

These three configurations were loaded to approximately the same nominal structural stress. At very low loads nonlinear behavior between strain and load was observed; this was attributed to the manner of load introduction into the test specimen. When the structural load was increased, all strains exhibited essentially a linear dependence upon load. The slopes of the linear portions were determined, and an average value for each pair of strain gages was obtained for each location. These average values of the slopes were assumed to be characteristic for the full strain-load behavior of the specimens. The values of strain given in Table 3 for various locations on the test specimen were calculated at the same nominal stress level.

A comparison of the strain values in Table 3 indicated that bending was induced through the thickness of the structural component under the crack gage. Also slight reverse bending occurred at the structural crack location. These bending effects are attributable to the asymmetrical specimen configuration. The strain values for the thicker structural component indicated that induced bending still occurred but that the magnitude was reduced due to the higher bending rigidity of the structure.

A comparison of the strain in the gage to that in the structure revealed another reduction of strain in addition to the reduction caused by bending. This decrement of strain was due to various factors such as deformation of the adhesive, some slight initial curvature in the gage, and the gage not conforming to the deformed curvature of the structure. Note that the strain decrement existed when rivets were placed along the edge of the bonded area. These strain results are employed later in the model in order to quantify some of the variables in the load-transfer relationship existing between the gage and the structural component.

Note that a small variation in strain occurred at the intended location of the SCH. Thus, the interaction between the crack gage and the nominal stress at the SCH location is assumed to be minimal.

4. TEST RESULTS

All specimens in the test matrix (Table 1) were tested under constant-amplitude, tension-tension, and sinusoidal loading with $R = 0.1$. Measurements of the gage and structure crack lengths and number of cycles were taken periodically during the loading history until the crack extended to the edge of the component in either the gage or the structure. An additional specimen planned for the test matrix yielded no data because an undetected debonding of the adhesive occurred early in the test. All specimens were tested in an MTS closed-loop hydraulic system and crack lengths were measured to the nearest 0.001-in. with a Gaertner traveling microscope.

Typical sets of data for crack length as function of number of cycles are shown in Figure 3 for Tests 3 and 4. For each test the number-of-cycles was eliminated in order to obtain the structural crack length as a function of gage crack length. Figures 4-6 are plots of structural crack length, a_s , as function of gage half-crack length, a_g , for all test data. The nominal stress range, $\Delta\sigma$, for the structural component for each test, is noted in these figures. The subscript on $\Delta\sigma$ indicates the test number. In Test 4, laser-interferometric measurements of crack-surface displacements (IDG) were made for three crack lengths. This laser technique provides a method of evaluating the geometric factor in the expression for the stress-intensity factor. The use of the IDG data is discussed in the results section. A detailed description of this interferometric method is presented in Reference 12.

The development of the model for predicting the theoretical curves in Figures 4-6 is presented in the next section.

SECTION III
PREDICTIVE MODEL

A summary of basic concepts and assumptions which are discussed in detail in Reference 9 are presented here for completeness. A crack propagation law is needed to characterize the crack growth in both the gage and the structure. For this investigation the empirical relationship

$$\frac{da}{dN} = C(\Delta K)^m \quad (1)$$

is assumed to be valid over the range of loads experienced by both the gage and the structure. Other crack-growth laws which could be used are discussed in References 9,10. The number of cycles to achieve a prescribed crack length, a , can be obtained by integration of Equation 1, which results in

$$N = \int_{a_1}^a \frac{d\alpha}{C[\Delta\sigma \beta \sqrt{\pi\alpha}]^m} \quad (2)$$

where the range for the stress-intensity factor is given by $\Delta K = \Delta\sigma \beta \sqrt{\pi a}$, β denoting the geometric correction factor and a_1 being the initial crack length.

For a crack gage attached to a structure, it is assumed that the following relationship exists between the nominal stresses in the gage and those in the structure:

$$\sigma_g = \sigma_s f \quad (3)$$

where f is the load-transfer function. For Equation 3 and subsequent formulae, the subscripts g and s refer to the gage and structure, respectively. In general, the load-transfer function depends upon the geometry of both the structure and the gage, the combined geometry of the structure and the attached gage, the properties of the structural and gage materials, and the material used for the attachment. A trivial implication from

Equation 3 is that the gage and structural components undergo the same number of loading cycles. Thus, the number of cycles for crack growth is the same for the gage and structure.

Writing Equation 2 for the crack in the gage and the crack in the structure and equating the number of cycles, the following expression is obtained:

$$\int_{a_{s1}}^{a_s} \frac{d\alpha}{C_s [\Delta\sigma_s \beta_s \sqrt{\pi\alpha}]^{m_s}} = \int_{a_{g1}}^{a_g} \frac{d\alpha}{C_g [\Delta\sigma_g \beta_g \sqrt{\pi\alpha}]^{m_g}} \quad (4)$$

which is a nonlinear expression relating crack lengths, material properties, and nominal stresses. Equation 4 can be simplified somewhat. For certain materials or certain alloys of the same basic material, the exponent m , in Equation 1 is approximately the same. Letting $m_s \approx m_g = m$ and substituting Equation 3 (for the range of nominal gage stress) into Equation 4, the relation between gage and structural crack lengths becomes independent of stresses; thus,

$$\frac{1}{C_s} \int_{a_{s1}}^{a_s} \frac{d\alpha}{[\beta_s \sqrt{\pi\alpha}]^m} = \frac{1}{C_g} \int_{a_{g1}}^{a_g} \frac{d\alpha}{[f \beta_g \sqrt{\pi\alpha}]^m} \quad (5)$$

This relation is used to predict the dependence of structural crack growth upon gage crack growth.

Determination of the material properties in Equation 5 which characterize baseline crack-growth behavior was discussed in the previous section. Since the exponents for crack-growth behavior are assumed to be equal for the theory, the exponent for the structural material, m_s , was arbitrarily chosen as the value for m . Then C_g for 7075-T6 and 2024-T3 was determined in order to achieve a least-squares fit to the experimental data. The adjusted values of C_g for the theory are given in Table 2.

For determination of the load-transfer function, the following analysis was made on a simplified model of the region of the structural component where the crack gage was located. The stress field, σ'_s , in the structure was assumed to vary linearly through the thickness under the center of the gage.

$$\sigma'_s(y) = T - \gamma My$$

where T , M , and γ are constants. The y -axis has its origin at the midplane of the structural component and is directed toward the gage. The constant γ is a factor which is intended to account for three-dimensional variations in the stress distribution, σ'_s , in the structural component under the crack gage. Its value is experimentally determined.

If P_g is assumed to be the internal force in the gage and P_s the externally applied force at the ends of the structure acting through the midplane, then the equilibrium of forces and of moments, respectively, produces the following expressions,

$$P_g + \int_{A_s} \sigma'_s dA = P_s \quad (6a)$$

$$P_g \left(\frac{B_s}{2} + B_a + \frac{B_g}{2} \right) + \int_{A_s} y \sigma'_s dA = 0 \quad (6b)$$

where A_s and B_s are the cross-sectional area and thickness, respectively, of the structural component and B_a and B_g represent the thickness of the adhesive and of the gage, respectively. Consideration of continuity of displacements between the gage and the top of the structure yields the expression

$$e_g P_g + e_a P_g = \frac{L_s}{E_s} \sigma'_s \left(y = \frac{B_s}{2} \right) \quad (6c)$$

where e_g is the compliance of the crack gage, e_a is a compliance which includes the compliance of the adhesive and other factors causing additional displacements between the gage and the structure, l_s is a characteristic length of the structural component under the crack gage, and E_s is Young's modulus of the structure. The right-hand side of (6c) represents the change in length along the surface of the structural component under the crack gage. The value of compliance, e_a , in (6c) is determined from the strain-gage results which were discussed in the previous section.

Equation 6 contains three unknowns--T, M, and P_g . Using the integration of the terms in Equation 6 and the definitions $\sigma_g \equiv P_g/A_g$ and $\sigma_s \equiv P_s/A_s$ for Equation 3, the load-transfer function can be written as

$$f = \frac{1}{E_s} \frac{l_g}{A_g} [e_g + e_s + e_a + \gamma e_b]^{-1} \quad (7)$$

where A_g is the cross-sectional area of the gage, e_s is the compliance of the structural component, and e_b is a bending compliance (the formula for e_b is given in the following discussion).

Evaluation of the compliances e_g , e_s , e_a , and e_b and the factor γ will now be presented. For the crack gage the expression relating compliance for a CC specimen, strain-energy release rate, and stress-intensity factor for plane stress is

$$\frac{1}{4} \frac{P^2}{B} \frac{\partial C}{\partial a} = G = \frac{K^2}{E}$$

After integration, the crack-gage compliance can be expressed as

$$\frac{1}{4} \frac{P^2}{B} (e_g - e'_g) = \frac{1}{E} \int_0^a K_B^2 da$$

where $e'_g = l_g / (E_g A_g)$ is the uncracked gage compliance. Substitution of the expression $K_g = \sigma_g \beta_g \sqrt{\pi a_g} = P_g \beta_g \sqrt{\pi a_g} / A_g$ yields

$$e_g = e'_g + \frac{4\pi B_g}{EA_g^2} \int_0^{a_g} \alpha \beta_g^2 d\alpha$$

For the crack-gage geometry used in the tests, the geometric correction factor is given in Reference 13. From the solution of Equation 6, the expressions for the structural compliance and the bending compliance are

$$e_s = \frac{l_s}{E_s A_s}$$

$$e_b = \frac{l_s B_s}{2E_s I_s} \left(\frac{B_s}{2} + B_a + \frac{B_g}{2} \right)$$

where I_s is the moment of inertia of cross section, A_s , of the structural component.

The values of the two remaining terms, C_a and γ , are determined from the experimental strain-gage results, Table 3. If the deformation of the uncracked gage ideally followed the deformation of the structure, the strain in the mid-section of the gage would be obtained by the linear continuation of the strain field in the structure. The value of C_a is calculated to account for the difference between the continuation of the strain field and the measured strain value. The value of γ is determined such that the assumed linear-strain distribution, $\epsilon'_s = \sigma'_s / E_s$, matches the measured strain values on the top and bottom of the structural component. As a result of these calculations, the following values are obtained for the terms in the load-transfer function for the test configuration in Figure 1: $e'_g = 2.51 \times 10^{-6}$ cm/N, $e_s = 0.163 \times 10^{-6}$ cm/N, $C_a = 0.171 \times 10^{-6}$ cm/N, $e_b = 0.588 \times 10^{-6}$ cm/N, and $\gamma = 0.3$.

The effect of the above quantities in the load-transfer function upon the predicted relation between a_s and a_g as given by Equation 5 is illustrated in Figure 7. The ideal behavior of a crack gage (Reference 9)

which undergoes the nominal deformation of the structure is given by curve a in Figure 7. For the ideal behavior the only term in brackets in the load-transfer function (Equation 7) is \mathcal{C}_g . Curves b through d are associated with successive inclusion of the compliances \mathcal{C}_s , \mathcal{C}_a , and $0.3 \mathcal{C}_b$, respectively. Curve e, like d, is obtained through the use of all the terms in brackets in Equation 7 except $\gamma = 1$.

The theoretical curves in Figures 4-6 are predicted from Equation 5, with $\gamma = 0.3$ in Equation 7. For the crack in the structural component, the geometric correction factor for the left-hand side of Equation 5 is calculated as

$$\beta_s = \beta_H \sec [(a_s + D)/W_s] \quad (8)$$

where β_H is the Bowie geometric factor for a single crack at a hole of diameter, D , in an infinite plate and W_s is the width of the structural component.

SECTION IV
DISCUSSION OF RESULTS

Prior to discussion of the measurements and the numerical predictions of the structural crack length and corresponding gage crack length, experimental measurements of the structural and the gage stress-intensity factors will be compared with values used in the numerical predictions. The stress-intensity factors are calculated from

$$K_s = \sigma_s \beta_s \sqrt{\pi a_s} \quad (9a) \quad K_g = \sigma_s f \beta_g \sqrt{\pi a_g} \quad (9b)$$

where β_s is given by Equation 8 and σ_g was eliminated by the use of Equation 3. Dimensionless forms of K are presented as a function of dimensionless crack length for the structural flaw in Figure 8* and for the center crack-gage geometry in Figure 9. These experimental results were obtained through the use of two procedures. First, the fatigue-crack-growth rates for the gage and structural cracks were converted to stress-intensity factors by means of Paris' crack-growth model previously established for the test material (Table 2). The second experimental K calibration method employed laser-interferometric measurements of crack surface displacement following the technique described in Reference 12.

The constants C and m used to convert the gage-crack-growth rates to K by the first technique were the values originally established during the baseline testing for the two-gage materials. In all cases, care was taken to ensure that the computed value of K from the measured gage and structural crack-growth rates fell within the linear range on a log-log scale of da/dN versus ΔK established in the baseline tests. Since the crack-growth models

*Note that the maximum value of the nondimensional crack length in Figure 8, i.e., when the crack reaches the edge of the structural component, is 0.375.

were not extrapolated, the only stress-intensity-factor data shown in Figures 8 and 9 are those for crack-growth rates within the baseline da/dN ranges. Since practically all of the structural and gage crack-growth rates fell within the baseline da/dN range tested, very few points were omitted.

Note in Figure 8 that the dimensionless K values which are equivalent to values of β_s in Equation 9a for the structural crack geometry form a very narrow scatter band. For the majority of the structural crack lengths (i.e., $a_s/W_s < 0.25$), the width-corrected Bowie geometric factor (Equation 8) agrees quite well with the experimental values, further verifying the assumption that placement of the gage on the structural member has no effect upon structural crack growth. The apparent divergence for a_s/W_s larger than 0.25 evidently indicates that the approximate width-corrected Bowie solution overcorrects for larger crack lengths.

Results of corresponding measurements of the dimensionless stress-intensity factor are given in Figure 9 for all of the center-cracked gages including both the 7075-T6 (Tests 1-4) and the 2024-T3 (Test 7) material. From Equation 9b the dimensionless stress-intensity factor in Figure 9 is equivalent to $\beta_g f \sqrt{a_g/W_g}$. Note that the dimensionless K for the 2024-T3 gages agrees well with the measured results for the 7075-T6 gages, as expected. There is considerably more scatter in the gage stress-intensity factors than in those in Figure 8 for the structural cracks. This increased scatter might be expected due to the potential variability of loads in the gage. The load must be transferred to the crack gage through an adhesive, for example, which introduces some variation in the geometry from test to test. Nevertheless, Equation 9b predicts gage stress-intensity factors which agree quite well with the experimental results, adding further confidence in the load-transfer model developed previously for the gage. The IDG results for the crack gage in Test 4 do not agree as well with the calculated dimensionless K results as do those obtained for the structural crack. At present the slightly different trend in the IDG results in comparison with the dimensionless K results is unexplainable.

Notice the agreement between experiment and theory in the gage-crack-versus-structural-crack results and the corresponding predictions for the six experiments presented in Figures 4-6. It is significant that the predictions required no knowledge of the actual loads applied to the test specimens. Although the agreement between predictions and test results for Tests 1-3 are not so good as those for Tests 4, 6, and 7, agreement between theory and experiment is still satisfactory for these cases. Possible sources of error will be discussed later.

Comparison of the result of Tests 2 and 3, which were initiated with approximately the same structural and gage initial crack lengths and approximately the same applied loads (Table 1) shows that the two tests have fairly reproducible results. A comparison of the results of Tests 2 and 3 with those of Test 4, again initiated with approximately the same initial crack lengths but at an appreciably higher stress level ($\Delta\sigma_4 = 124$ MPa rather than ~ 94 MPa) shows the structural-crack-length-versus-gage-crack-length data to be essentially independent of load level, with the data from all three tests falling within a relatively narrow band (Figure 10). Figure 3 which presents the original crack-length-versus-number-of-cycles data for Tests 3 and 4 demonstrates that load level does, of course, influence the cyclic life of otherwise identical specimens; however, as shown in Figure 10, load level had no appreciable effect upon the a_s -versus- a_g curve.

This observation is in agreement with the mathematical model which led to the conclusion that these curves were independent of loading when crack-growth data could be expressed by a simple Paris-type model. Since as discussed in prior papers (References 9, 10, 14, 15), crack-growth data due to variable-amplitude loading can often be described by such a model (i.e., correlating crack growth per block of loading with an appropriate stress-intensity factor which characterizes the loading block), the results of these constant-amplitude tests suggest that--with limitations--crack gages may also be useful for variable-load histories characteristic of actual structures. In References 9,10 correlations were made between the growth of two flaws in the same test specimen using the present computational

technique. The gage in this case was considered to be an integral part of the structure. Those predictions which were again independent of load history, being a function of geometric and material variables only, agreed extremely well with results on experimental behavior when the test specimens were subjected to a complex variable-amplitude-load profile chosen to simulate aircraft loading.

One source of the discrepancy between prediction and experiment observed for Tests 1-3 may be the variability in gage fatigue-crack-growth rate caused by relative humidity changes. The crack gages for these three experiments were made from 7075-T6 aluminum, an alloy which is particularly susceptible to such environmental influences (Reference 16). Since no attempts were made to control the test environment, perhaps some of the scatter for the 7075-T6 gages evident in the stress-intensity-factor measurements in Figure 9 and in the predictions of the a_s -versus a_g data for Tests 1-3 is due to changes in test humidity. These tests were conducted during the summer months when problems developed with the laboratory air-conditioning system and rather large, although unmeasured, changes in ambient temperature and humidity occurred. Consistent with this observation is the fact that the data for the 2024-T3 gages showed excellent agreement with theory. The 2024-T3 alloy is much less sensitive to environmental changes than the 7075-T6 material.

SECTION V
SUMMARY AND CONCLUSIONS

The crack-growth gage has been discussed as a potential technique for monitoring structural loads in order to determine their influence upon the growth of possible structural cracks. Briefly stated, the concept consists of mounting a precracked coupon (or gage) onto a load-bearing structural member. The coupon receives the load excursions which are related to the loads in the structure by the transfer function (Equation 3) and responds with a measurable crack extension. This crack growth in the gage may be correlated with extension of another defect located in the structural member by means of the techniques described here and in prior papers (References 9,10). In essence, the cracked coupon acts as an analog computer which senses the load history, determines its effect upon crack growth, and responds with a measurable output (gage crack extension).

A mathematical technique for relating the gage crack length and the structural crack length has been described. The present model is an improvement over earlier versions (References 9,10) and takes into account such factors as local reinforcement or bending caused by the crack gage and compliance of the adhesive bond. Predictions of crack-gage response were made by means of this model and subjected to experimental verification. Six crack-gage tests were conducted involving two different gage materials, two load levels, and two gage geometries. The mathematical predictions agreed well with results on the observed experimental behavior of the crack gages. Reproducibility in response of identical gages was demonstrated and preliminary verification was obtained concerning correlation between gage crack growth and flaw growth in the structure being independent of load history. Although this conclusion is limited in the present tests to constant-amplitude loadings, there is evidence (References 9,10) to suggest that these findings may apply to more complex load histories which can be described by simple Paris-or Foreman-type crack-growth models. Verification of the concept and identification of its limitations for variable-amplitude loading require further study.

No attempts were made here to optimize the crack-gage design for structural applications. Efforts were directed instead toward experimentally evaluating the crack-gage concept for load tracking. Improved gage geometries, for example, can almost certainly be developed, along with selection of alternate adhesives for better long-term durability and structural application. Although the present results indicate that predictions can be made for crack gages made of materials which are different from those used for the structural member, it might be desirable to use identical materials in order to obtain similar retardation effects caused by peak loads. Similar materials would also minimize differences in the environmental effects upon crack-growth rates encountered by the gage and structure in service. One final consideration which may be important in optimizing the gage design lies in the initial crack lengths and the precracking procedures used to introduce the gage flaw. For instance, perhaps the precracking loads should be less than service loads in order to minimize history effects in the gage. It may also be desirable to select an initial gage crack length leading to stress-intensity-factor excursions in the gage which are of similar magnitude to those seen by the structural defect.

Thus, in summary, the authors feel that the present results demonstrate the potential of crack-growth gages for monitoring service loads. The fact that an accurate relationship between gage and structural crack length can be predicted in advance (with no knowledge of subsequent load history and being dependent only upon geometric and material parameters) suggests that the crack gage is an extremely simple and useful device for recording and interpreting the effect of service usage upon possible structural crack growth. Although many steps remain in the development of a working device for a given service application, it would appear that potential problems are readily solvable by means of present engineering methods. We suggest that other investigators give the crack-gage concept serious consideration for their load-monitoring needs and encourage their research and development efforts on this interesting technique for fleet tracking.

REFERENCES

1. M. D. Coffin and C. F. Tiffany, "New Air Force Requirements for Structural Safety, Durability, and Life Management," Journal of Aircraft (AIAA), Vol. 13, No. 2, 1976, pp. 93-98.
2. "Aircraft Structural Integrity Programs, Airplane Requirements," Military Standard MIL-STD-1530A (11) (USAF), 11 December 1975.
3. "Airplane Damage Tolerance Requirements," Military Specification MIL-A-83444 (USAF), 2 July 1974.
4. T. T. King, "Some Developments in the Air Force Aircraft Structural Integrity Program (ASIP)," AFFDL-TR-70-144, Proceedings of the Air Force Conference on Fatigue and Fracture of Aircraft Structures and Materials, ed. H. A. Wood et al., Air Force Flight Dynamics Laboratory, Wright-Patterson Air Force Base, Ohio, 1970, pp. 701-721.
5. D. H. Whitford and R. J. Dominic, "B-58 Fleet Life Monitoring and Usage Evaluation by Cumulative Fatigue Damage Method," AFFDL-TR-70-144, Proceedings of the Air Force Conference on Fatigue and Fracture of Aircraft Structures and Materials, ed. H. A. Wood et al., Air Force Flight Dynamics Laboratory, Wright-Patterson Air Force Base, Ohio, 1970, pp. 847-864.
6. D. R. Harting, "The - S/N - Fatigue-Life Gage: A Direct Means of Measuring Cumulative Fatigue Damage," Experimental Mechanics, Vol. 6, No. 2, February 1966, pp. 19A-24A.
7. J. C. Spanner and E. McElroy, Monitoring Structural Integrity by Acoustic Emission, ASTM STP 571, American Society for Testing and Materials, 1975.
8. H. W. Smith, Fatigue Damage Indicator, U. S. Patent No. 3, 979, 949, assigned to The Boeing Company, Seattle, Washington, September 14, 1976.
9. A. F. Grandt, Jr., R. L. Crane, and J. P. Gallagher, "A Crack Growth Gage for Assessing Flaw Growth Potential in Structural Components," Fracture, Proceedings of the Fourth International Conference on Fracture, Waterloo, Canada, 19-24 June 1977, Vol. 3, pp. 39-45.
10. J. P. Gallagher, A. F. Grandt, Jr., and R. L. Crane, "Tracking Crack Growth Damage at Control Points," AIAA Paper No. 77-379 presented at the 18th Structures, Structural Dynamics, and Materials Conference, San Diego, California, 21-23 March 1977.
11. W. S. Johnson and S. J. Paquette, "Service Life Monitoring Coupons - Accounting for Potential Crack Growth in Fleet Aircraft," presented at the 18th SDM Conference AIAA/ASME, San Diego, California, March 21-23, 1977.

REFERENCES (CONTINUED)

12. D. E. Macha, W. N. Sharpe, Jr., and A. F. Grandt, Jr., "A Laser Interferometry Method for Experimental Stress Intensity Factor Calibration," Cracks and Fracture, ASTM STP 601, American Society for Testing and Materials, 1976, pp. 490-505.
13. M. Isida, "Effect of Width and Length on Stress Intensity Factors of Internally Cracked Plates under Various Boundary Conditions," International Journal of Fracture Mechanics, Vol. 7, 1971, pp. 301-316.
14. J. P. Gallagher and H. D. Stalnaker, "Developing Methods for Tracking Crack Growth Damage in Aircraft," Proceedings AIAA/ASME/SAE 17th Structures, Structural Dynamics, and Materials Conference, May 5-7, 1976, pp. 486-494.
15. S. T. Rolfe and J. M. Barsom, Fracture and Fatigue Control in Structures, Prentice Hall, Englewood Cliffs, N. J., 1977.
16. W. G. Truckner, J. T. Staley, R. J. Bucci, and A. B. Thakker, Effects of Microstructure on Fatigue Crack Growth of High Strength Aluminum Alloys, AFML-TR-76-169, Air Force Materials Laboratory, Wright-Patterson Air Force Base, Ohio, October 1976.

Table 1 - CRACK GAGE TEST MATRIX.^a

Test Number	Material	Gage Crack Geometry ^b	Initial Crack Lengths		Maximum Nominal Structural Stress (MPa)
			Gage (mm)	Structure (mm)	
1	7075-T6	CC	8.92	6.35	103
2	7075-T6	CC	5.08	1.27	105
3	7075-T6	CC	5.03	1.40	103
4	7075-T6	CC	5.08	1.30	138
6	2024-T3	SCH (3.18)	0.18	0.36	183
7	2024-T3	CC	15.7	1.32	103

^aAll structural material was 2219-T851 with SCH (6.35) except Test 6 with SCH (7.94).

^bCenter crack indicated by CC. Single-cracked hole indicated by SCH with hole diameter (in mm) given in parentheses.

Table 2 - CRACK GROWTH CONSTANTS FOR PARIS' LAW.

$$\frac{da}{dN} = C(\Delta K)^m$$

$$\left(\frac{da}{dN} - \text{m/cycle}; \Delta K - \text{MN m}^{-3/2}\right)$$

		Material		
		2219-T851 ^a	7075-T6 ^b	2024-T3 ^b
Adjusted Experimental	C	0.1450×10^{-9}	0.4278×10^{-9}	0.4621×10^{-10}
	m	2.855	2.816	3.13
	C	0.1450×10^{-9}	0.3867×10^{-9}	0.8810×10^{-10}
	m	2.855	2.855	2.855

^aNominal thickness - 0.61 cm

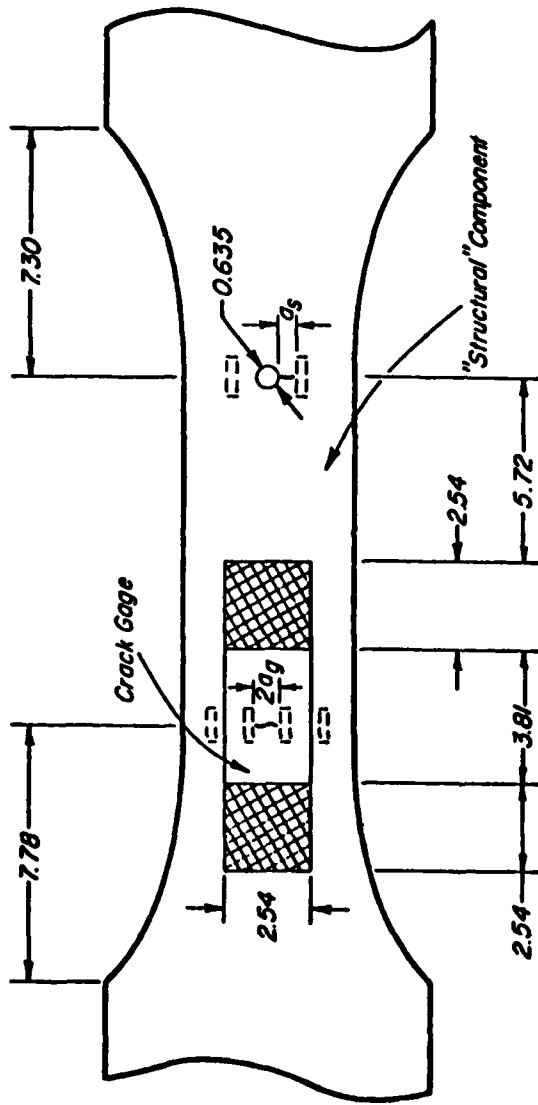
^bNominal thickness - 0.084 cm

Table 3 - STRAIN VALUES FOR UNCRACKED GAGE MOUNTED ON STRUCTURE WITH NO HOLE.

(Strains - 10^{-3} cm/cm)

	Adhesive Only ^a		Adhesive Plus Rivets	
	Crack Gage Location	Proposed SCH Location	Crack Gage Location	Proposed SCH Location
0.605-cm Thick Structure ($\sigma_g = 130$ MPa)				
Top of Gage	1.36	-	1.38	-
Top of Structure	1.45	1.75	1.44	1.77
Bottom of Structure	1.66	1.69	1.70	1.72
1.33-cm Thick Structure ($\sigma_g = 130$ MPa)				
Top of Gage	1.47	-		
Top of Structure	1.59	1.72		
Bottom of Structure	1.74	1.70		

^aIn all cases adhesive was Hysol EA 9628 tape.



Nominal Structure Thickness - 0.61
 Nominal Gage Thickness - 0.079
 Nominal Adhesive Thickness - 0.018

Strain Gages

Adhesive

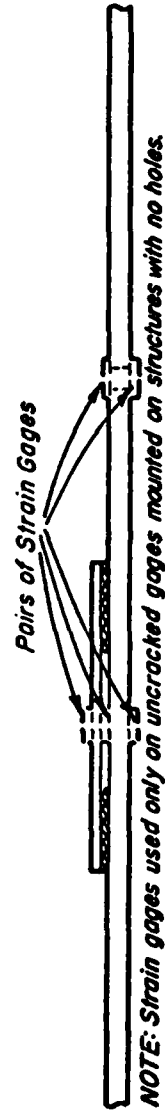


Figure 1. Test Spec Configuration or Configuration of TS

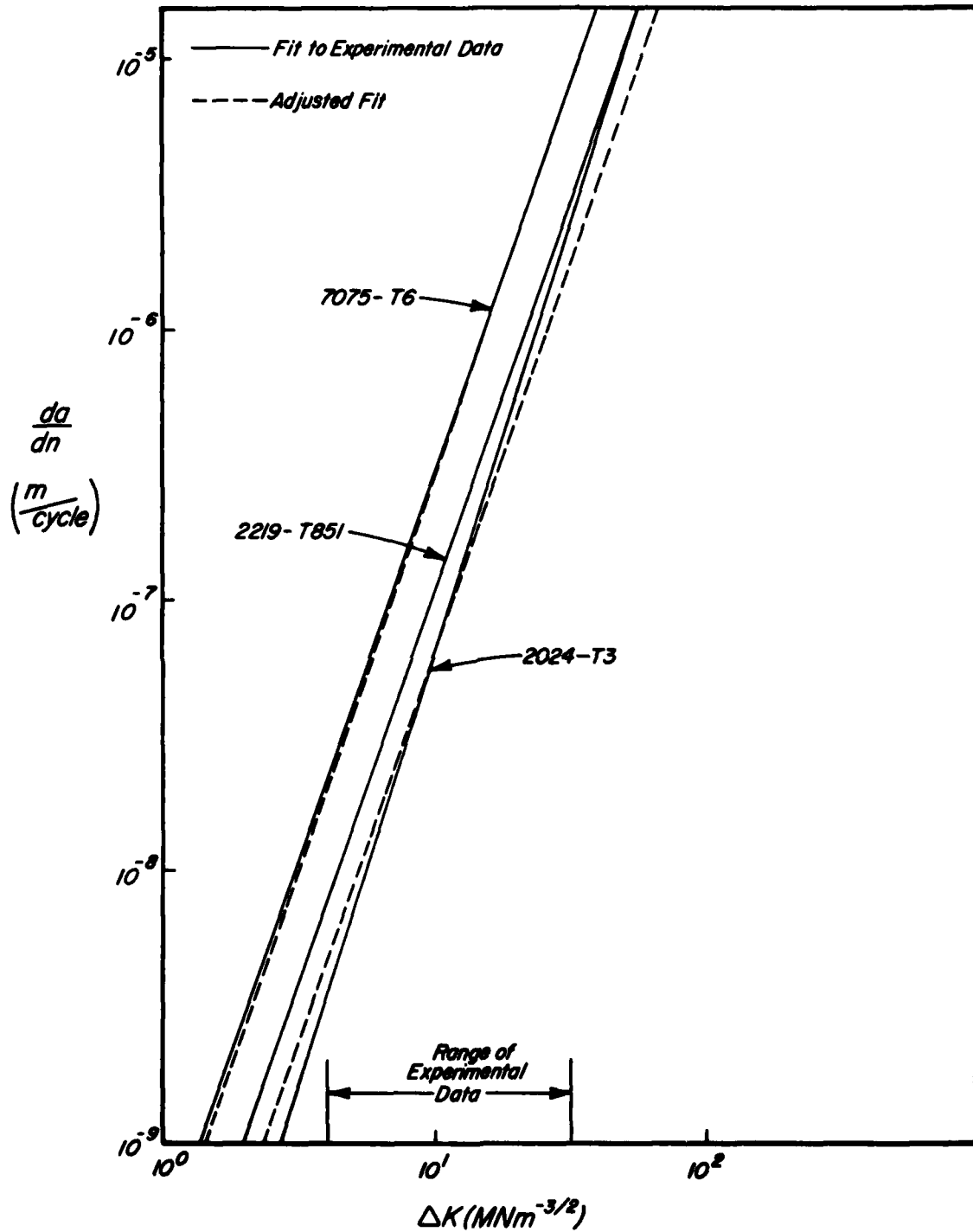


Figure 2. Plot of Predicted Crack Growth Behavior from a Best Fit to the Experimental Data and an Adjusted Fit to the Data

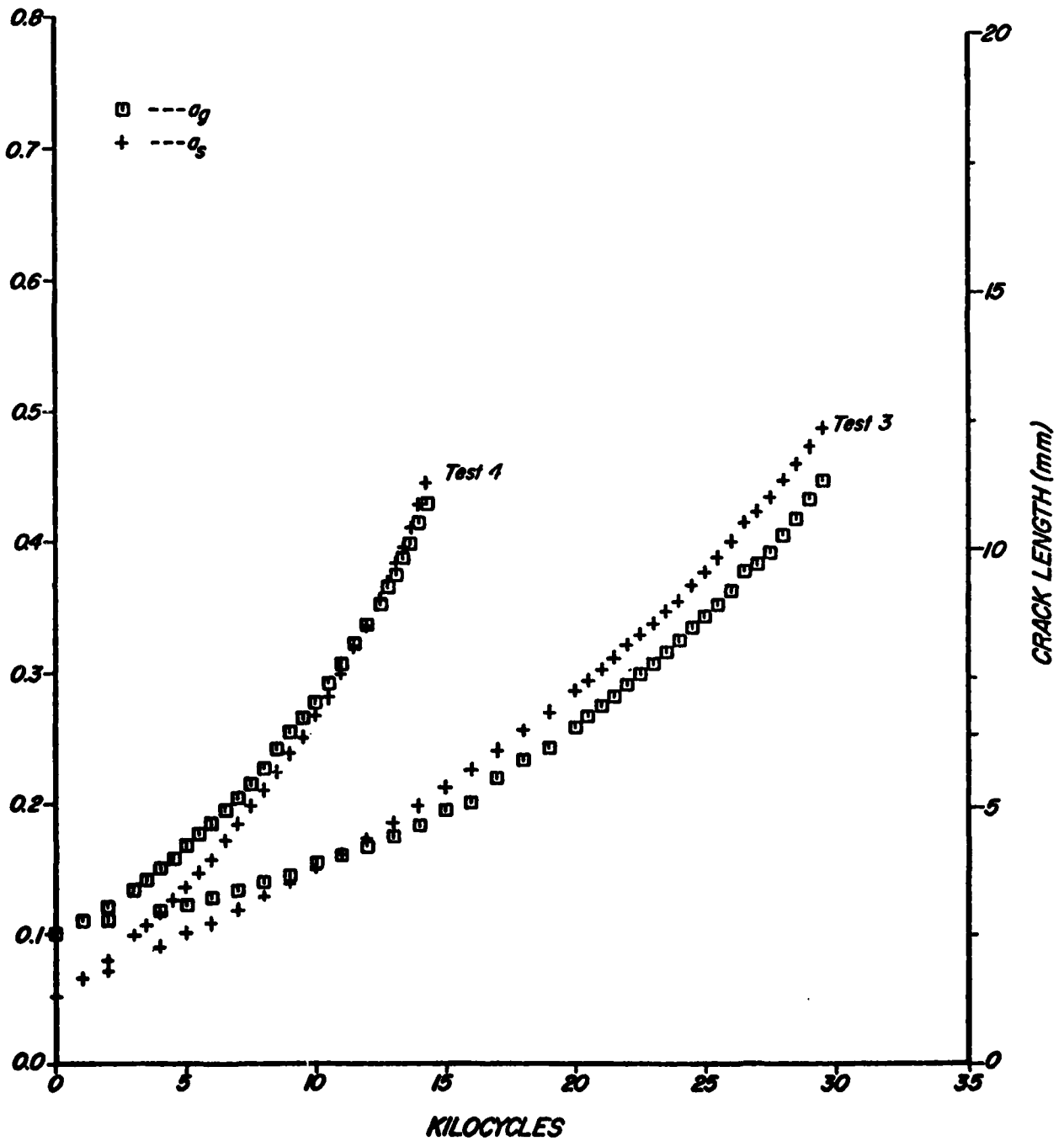


Figure 3. Comparison of Crack-Length Results for Two Specimens Having Equivalent Initial Crack Lengths and Being Tested Under Different Load Amplitudes

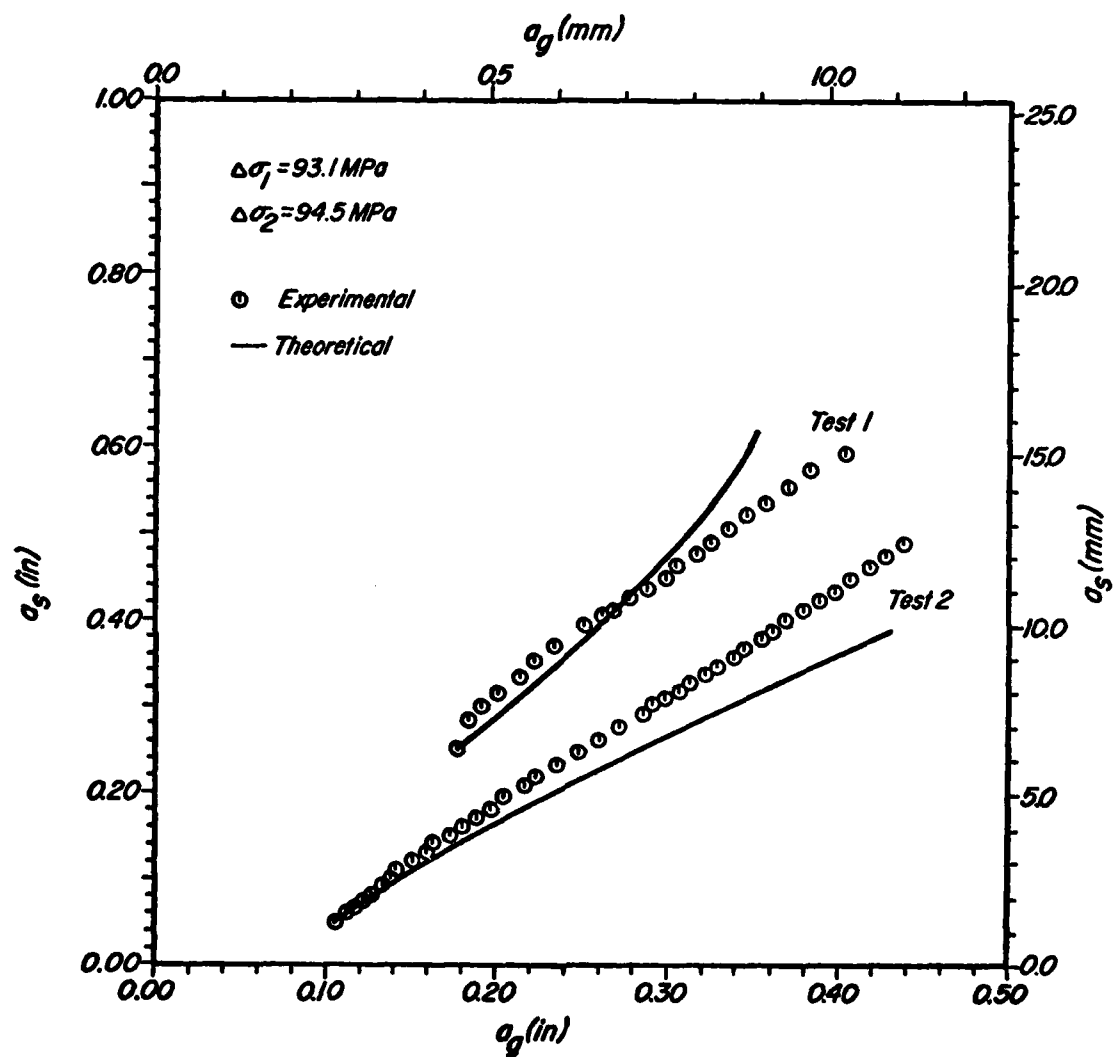


Figure 4. Experimental Data and Theoretical Predictions for Structural Crack Growth Versus Gage Crack Growth for Two Specimens Having Different Initial Crack Lengths

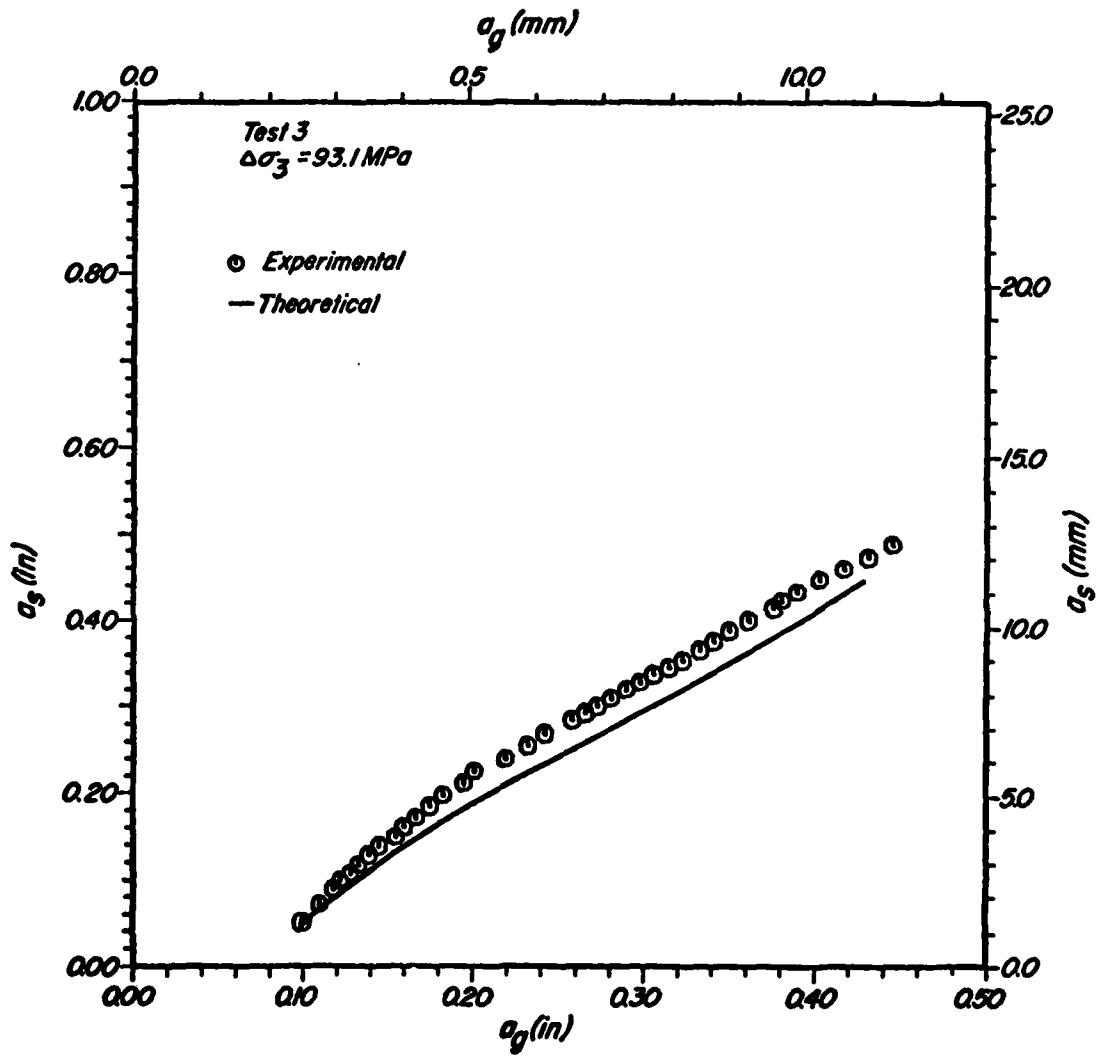


Figure 5a. A Replot of the Test Data in Figure 2 After Elimination of the Dependence Upon the Number of Cycles: Test 3 with Nominal Stress Range of 93.1 MPa

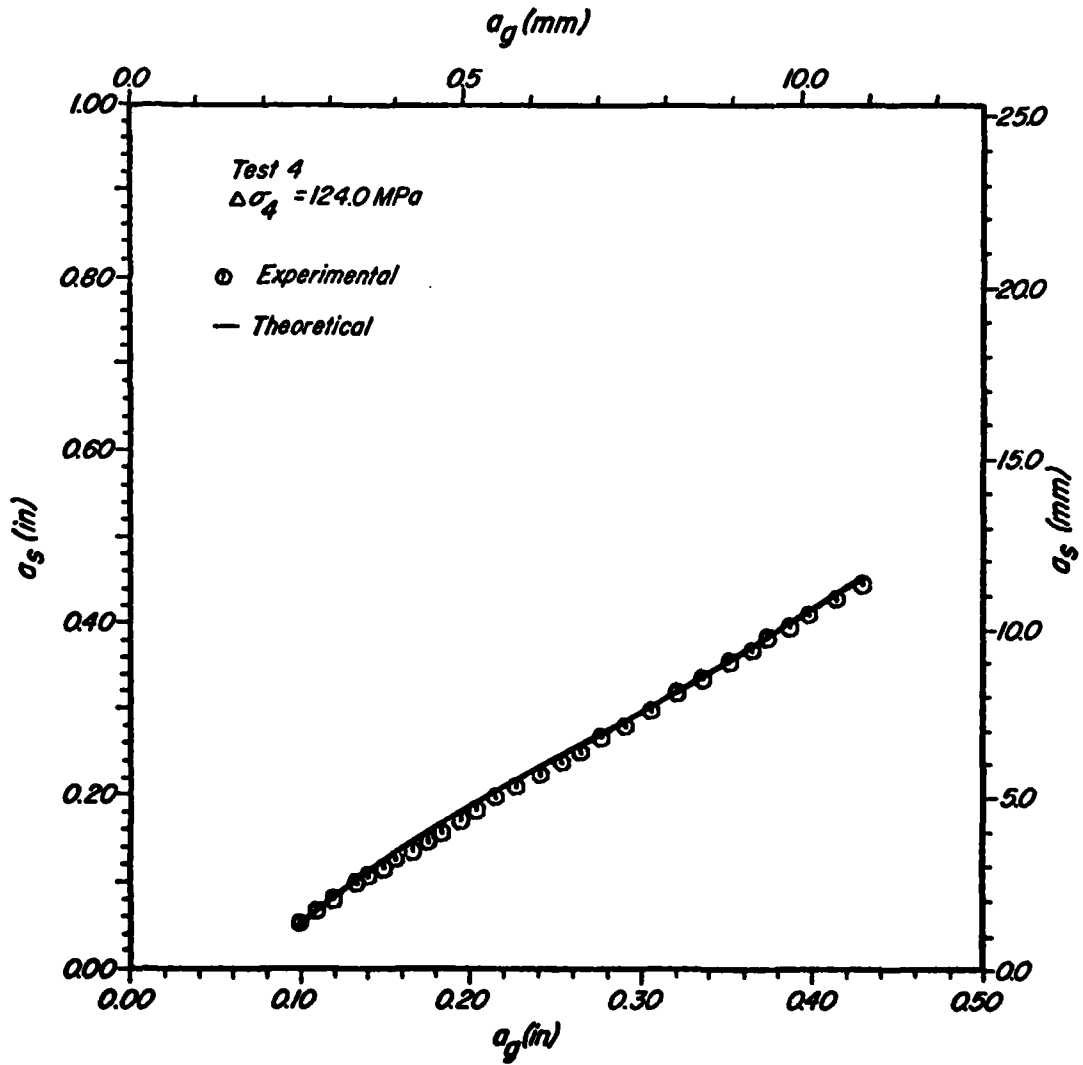


Figure 5b. A Replot of the Test Data in Figure 2 After Elimination of the Dependence Upon the Number of Cycles: Test 4 with Nominal Stress Range of 124 MPa

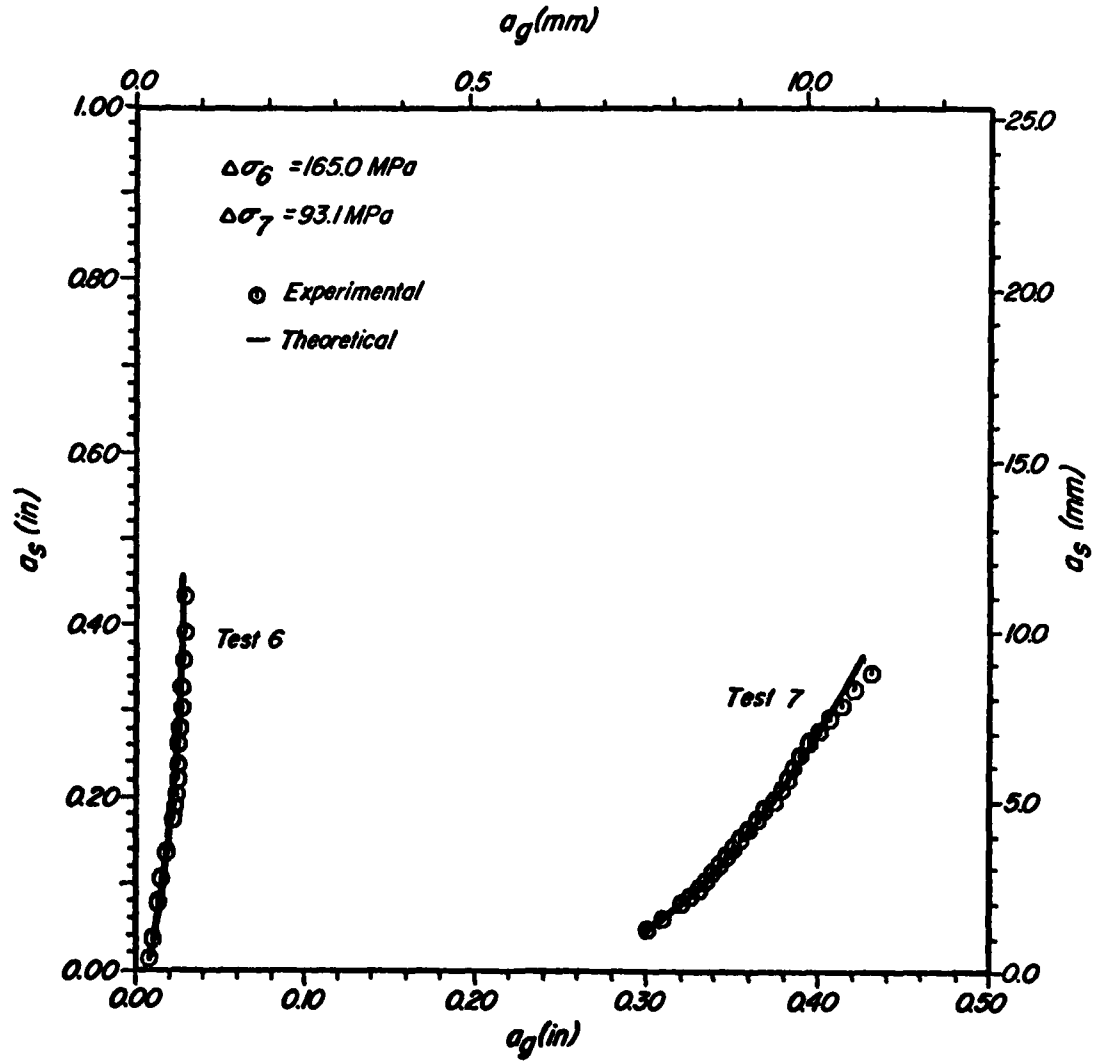


Figure 6. Plot of Structural Crack Length Versus Gage Crack Length for Specimens With Gages Made from 2024-T3 A1

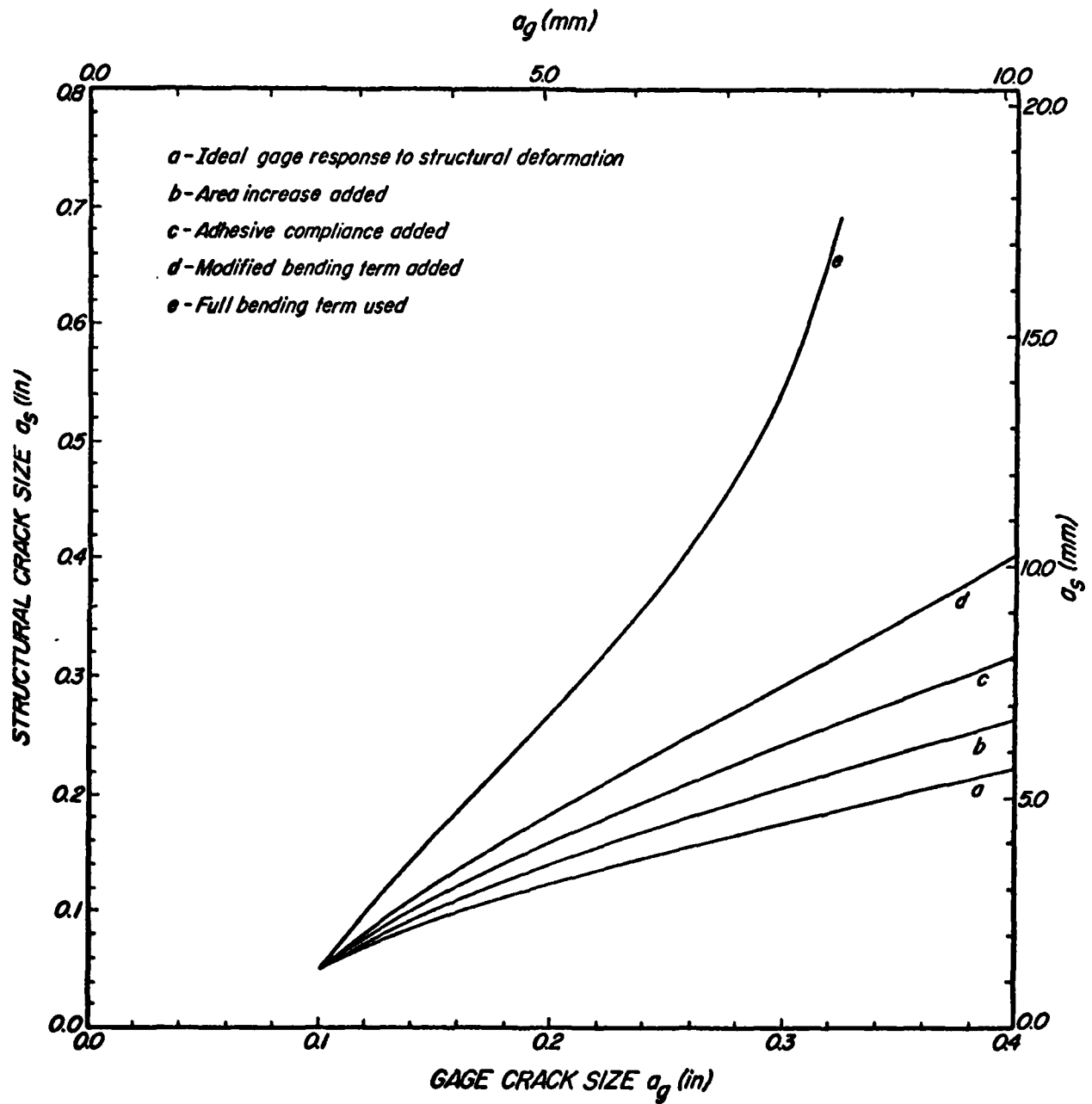


Figure 7. Cumulative Effect of Additional Compliance Terms in the Load-Transfer Function Upon the Prediction of Structural Crack Length Versus Gage Crack Length

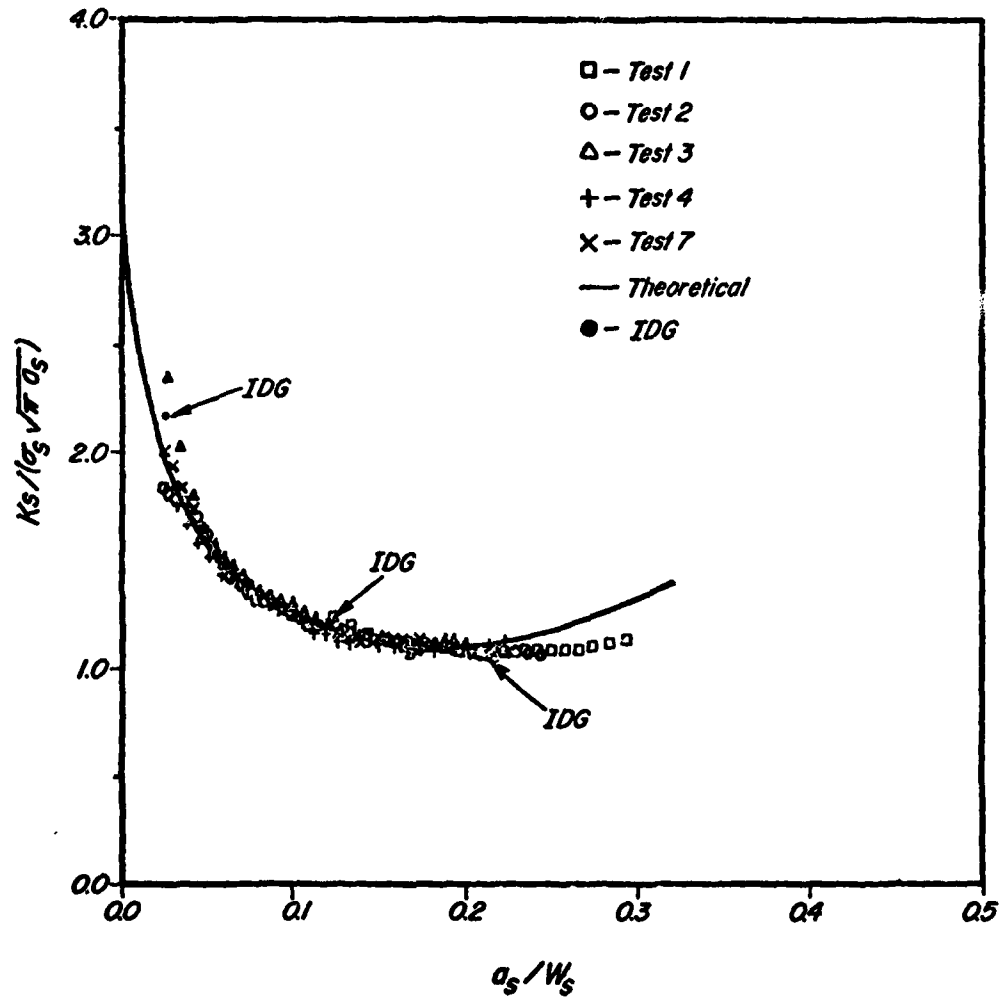


Figure 8. Comparison of the Predicted Dimensionless K--Equivalent to the Geometric Correction Factor--With the Dimensionless K Obtained from the Experimental Data on Structural Crack Growth

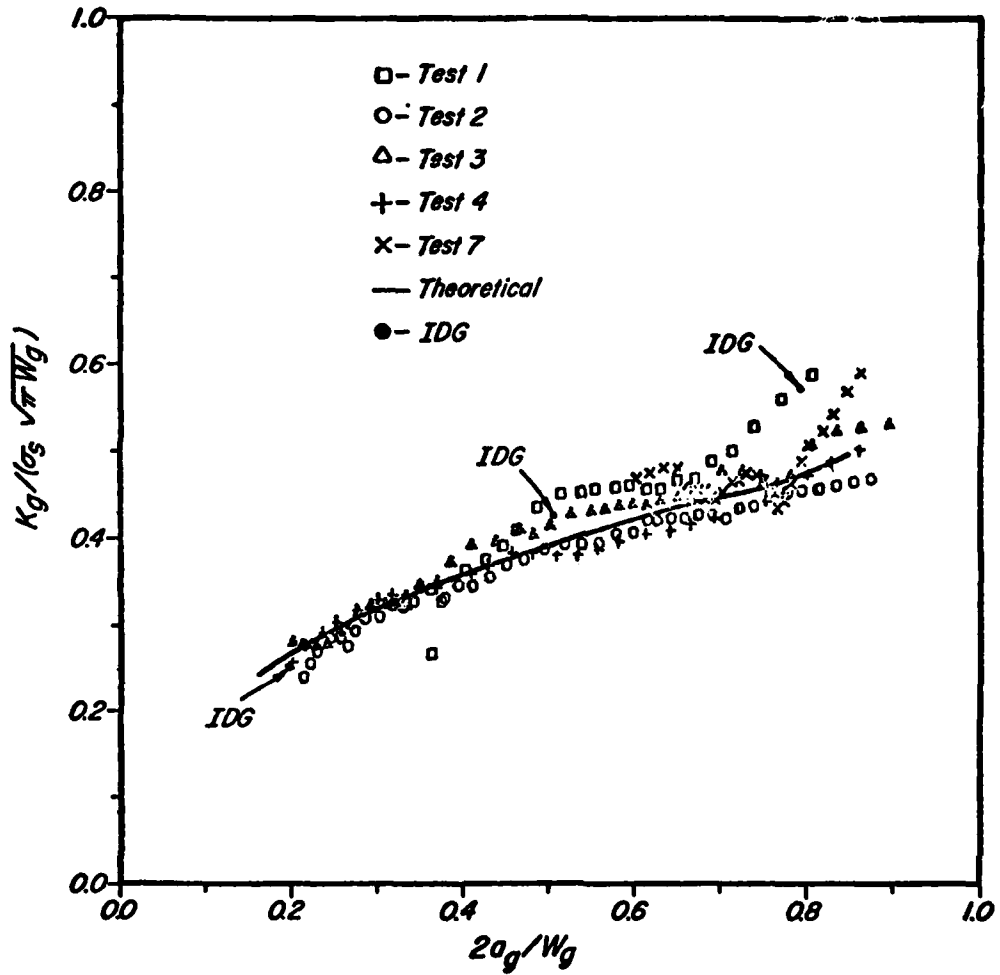


Figure 9. Comparison of the Predicted Dimensionless K--Equivalent to the Load-Transfer Function--With the Dimensionless K Obtained from the Experimental Data on Gage Crack Growth

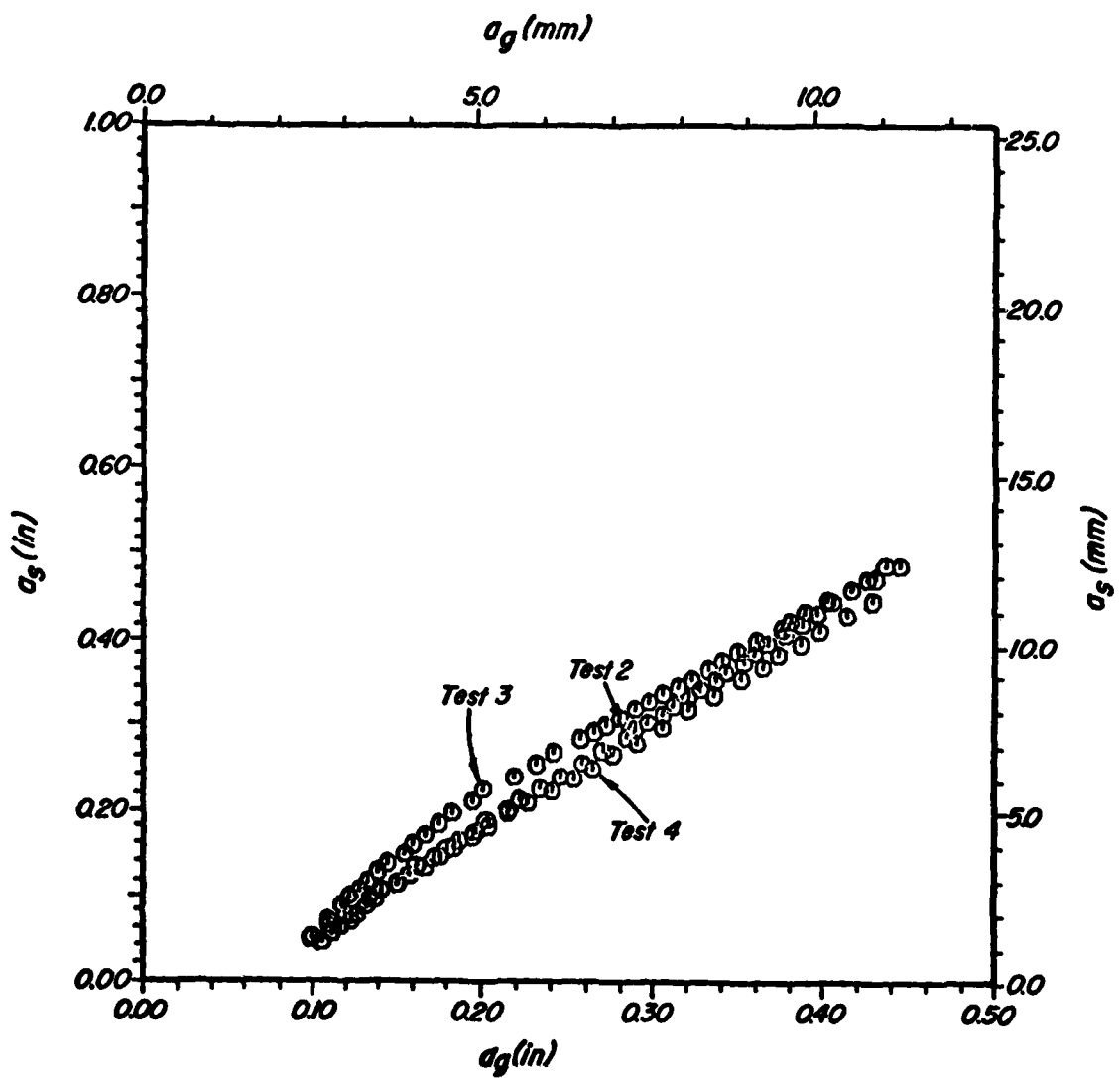


Figure 10. Experimental Crack-Growth Data Indicating Both the Reproducibility and the Lack of Dependence Upon Load Amplitude of the Gage Response

AFML-TR-77-233

APPENDIX

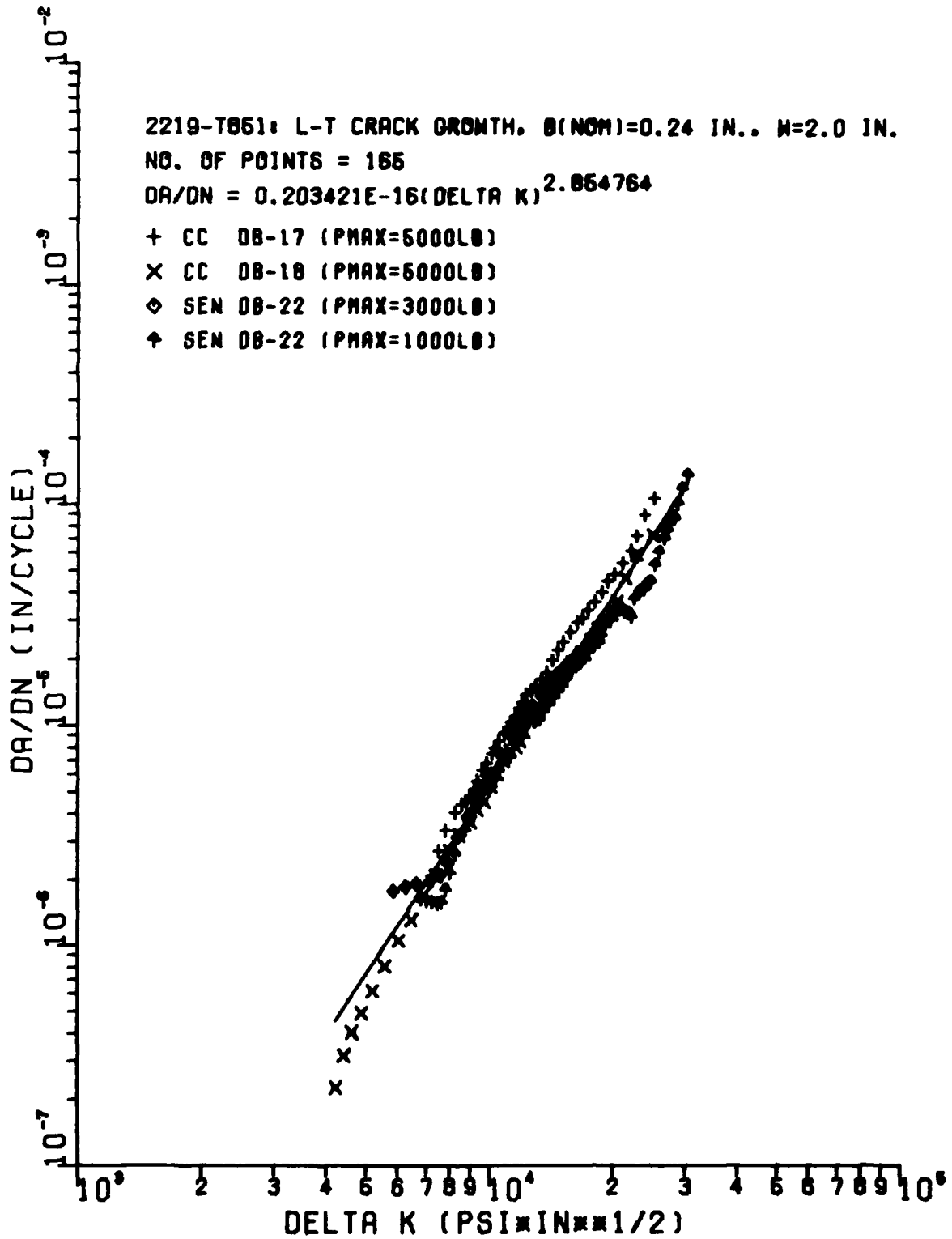


Figure A1. Crack Growth Rate for 2219-T851 Aluminum

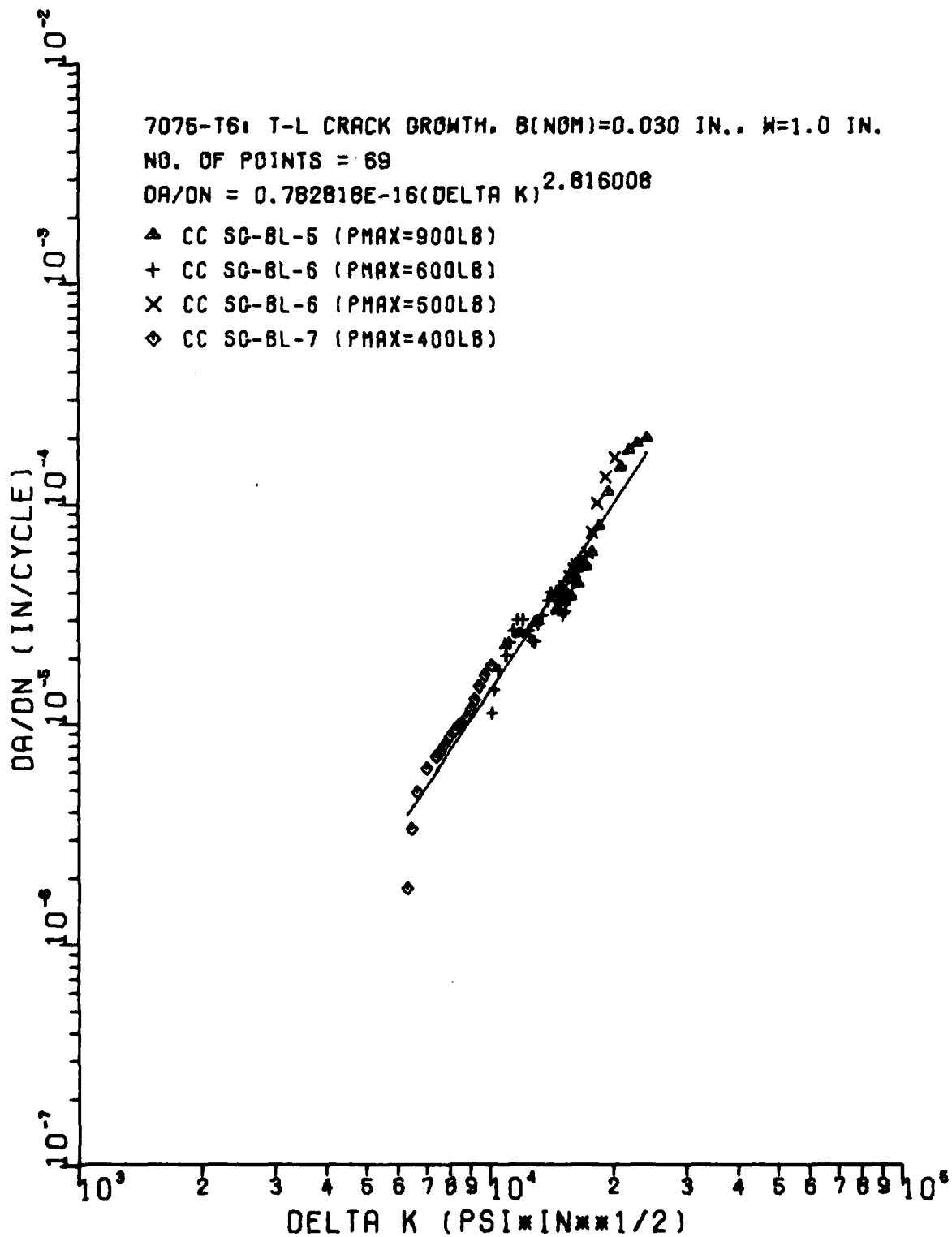


Figure A2. Crack Growth Rate for 7075-T6 Aluminum

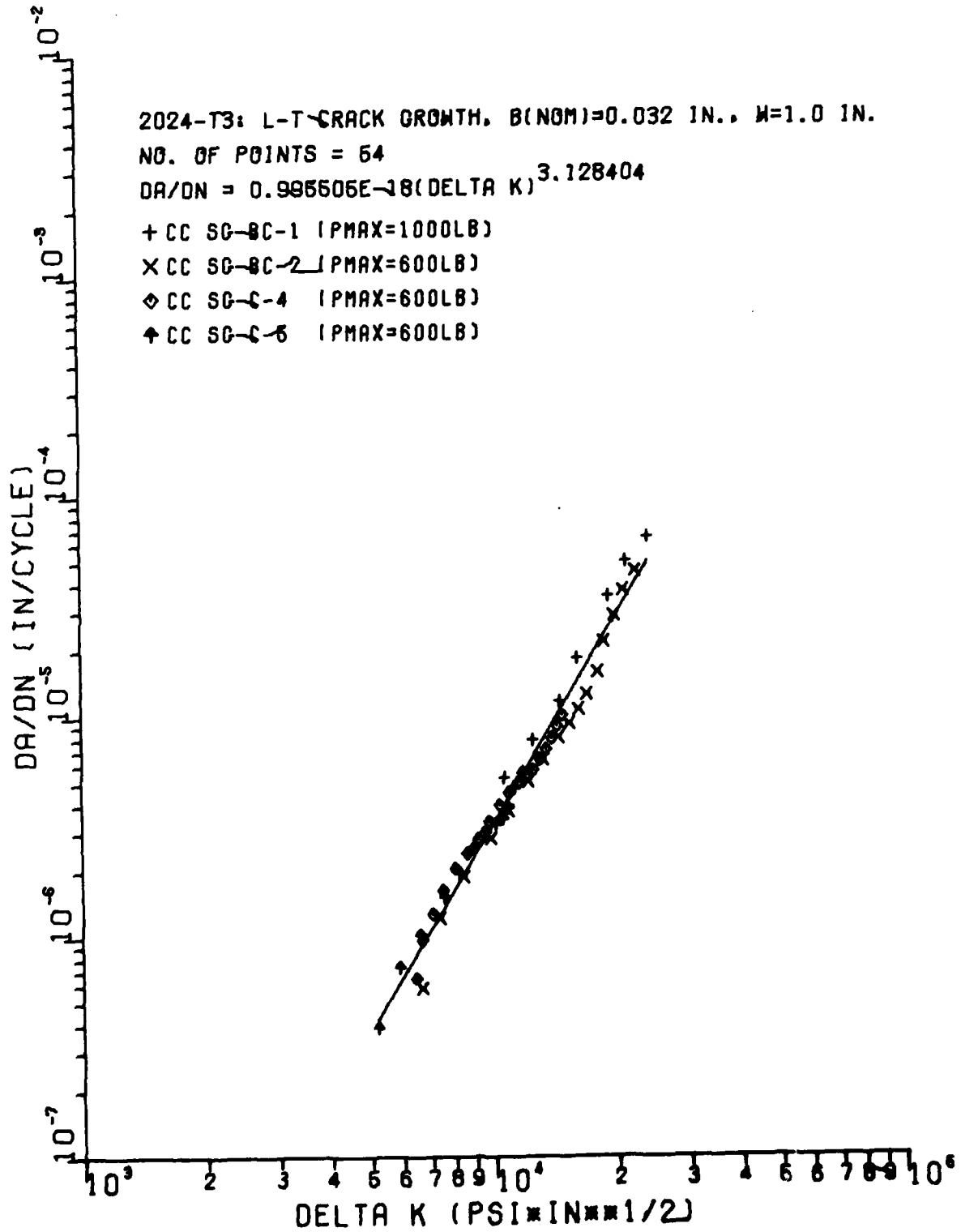


Figure A3. Crack Growth Rate for 2024-T3 Aluminum